PLOS COMPUTATIONAL BIOLOGY

RESEARCH ARTICLE

Understanding the high-order network plasticity mechanisms of ultrasound neuromodulation

Marilyn Gatica[1,2*], **Cyril Atkinson-Clement**[2,3], **Carlos Coronel-Oliveros**[4,5,6], **Mohammad Alkhawashki**[2], **Pedro A. M. Mediano**[7,8], **Enzo Tagliazucchi**[4,9], **Fernando E. Rosas**[10,11,12], **Marcus Kaiser**[2,13,14,15], **Giovanni Petri**[1,16,17]

1 NPLab, Network Science Institute, Northeastern University London, London, United Kingdom, **2** Precision Imaging, School of Medicine, University of Nottingham, Nottingham, United Kingdom, **3** Brain Research and Imaging Centre, Faculty of Health, University of Plymouth, Plymouth, United Kingdom, **4** Latin American Brain Health Institute (BrainLat), Universidad Adolfo Ibáñez, Santiago, Chile, **5** Global Brain Health Institute (GBHI), Trinity College Dublin, Dublin, Ireland, **6** Trinity College Dublin, Dublin, Ireland, **7** Department of Computing, Imperial College London, London, United Kingdom, **8** Division of Psychology and Language Sciences, University College London, London, United Kingdom, **9** University of Buenos Aires, Buenos Aires, Argentina, **10** Sussex Centre for Consciousness Science and Sussex AI, Department of Informatics, University of Sussex, Brighton, United Kingdom, **11** Department of Brain Science and Centre for Complexity Science, Imperial College London, London, United Kingdom, **12** Center for Eudaimonia and Human Flourishing, University of Oxford, Oxford, United Kingdom, **13** NIHR Biomedical Research Centre, University of Nottingham, Nottingham, United Kingdom, **14** School of Computing Science, Newcastle University, Newcastle, United Kingdom, **15** Rui Jin Hospital, Shanghai Jiao Tong University, Shanghai, China, **16** Department of Physics, Northeastern University, Boston, Massachusetts, United States of America, **17** CENTAI Institute, Turin, Italy

* marilyn.gatica@nulondon.ac.uk

Citation: Gatica M, Atkinson-Clement C, Coronel-Oliveros C, Alkhawashki M, Mediano PAM, Tagliazucchi E, et al. (2025) Understanding the high-order network plasticity mechanisms of ultrasound neuromodulation. PLoS Comput Biol 21(10): e1013514. https://doi.org/10.1371/journal.pcbi.1013514

Editor: Zhiyi Chen, Third Military Medical University: Army Medical University, CHINA

Received: May 22, 2025

Accepted: September 10, 2025

Published: October 6, 2025

Data availability statement: The data analysis was conducted using MATLAB version 2022b. The MATLAB code for quantifying synergy and redundancy from integrated information decomposition of time series, utilizing the Gaussian MMI solver, is available at https://doi.org/10.1038/s41593-022-01070-0. We computed the communication models for

Abstract

Transcranial ultrasound stimulation (TUS) is an emerging non-invasive neuromodulation technique, offering a potential alternative to pharmacological treatments for psychiatric and neurological disorders. While functional analysis has been instrumental in characterizing the TUS effects, understanding its indirect influence across the network remains challenging. Here, we developed a whole-brain model to represent functional changes as measured by fMRI, enabling us to investigate how TUS-induced effects propagate throughout the brain with increasing stimulus intensity. We implemented two mechanisms: one based on anatomical distance and another on broadcasting dynamics, to explore plasticity-driven changes in specific brain regions. Finally, we highlighted the role of higher-order functional interactions in localizing spatial effects of off-line TUS at two target areas—the right thalamus and inferior frontal cortex—revealing distinct patterns of functional reorganization. This work lays the foundation for mechanistic insights and predictive models of TUS, advancing its potential clinical applications.

weighted networks using the Brain Connectivity Toolbox: http://www.brain-connectivity-toolbox.net. We used the Python code to simulate the Hopf model, freely available at: https://github.com/carlosmig/StarCraft-2-Modeling.git. Brain plot visualizations were generated using MRIcroGL: https://www.nitrc.org/projects/mricrogl/. A Python code to reproduce this work, along with the data necessary to run the code, is available at https://github.com/nplresearch/Modelling-TUS.

Funding: M.K. and C.A., were supported by the Engineering and Physical Sciences Research Council (EP/W004488/1, EP/X01925X/1 and EP/W035057/1). M.K. was also supported by the Medical Research Council (UKRI 527), the NIHR Nottingham Biomedical Research Centre, and the Guangci Professorship Program of Rui Jin Hospital (Shanghai Jiao Tong University). G.P. acknowledges support from the European Research Council (ERC) Consolidator Grant under the European Union's Horizon Europe programme (grant agreement No. 101171380, project RUNES).The funders had no role in study design, data collection and analysis, decision to publish, or preparation of the manuscript.

Competing interests: The authors have declared that no competing interests exist.

Author summary

Transcranial ultrasound stimulation (TUS) offers a non-invasive approach to modulating brain activity, holding promise for treating psychiatric and neurological disorders. Despite its potential, the mechanisms underlying its effects remain poorly understood. By integrating human fMRI data with whole-brain computational models, we identified how high-order functional interactions localize and propagate TUS-induced effects from local to global brain scales. This work introduces two mechanisms—distance-based propagation and diffusion-like broadcasting—that predict functional plasticity changes, providing a foundation for understanding and optimizing the biological and cognitive outcomes of TUS. Our findings offer critical insights into the dynamics of neuromodulation, bridging experimental results and clinical applications.

Introduction

Non-invasive neuromodulation techniques have been gaining ground as an alternative to pharmacological interventions for the treatment of psychiatric and neurological conditions [1–3]. Existing tools can modulate neuronal firing rates via techniques including transcranial direct current stimulation, transcranial magnetic stimulation, and low-intensity transcranial ultrasound stimulation (TUS) — with the latter being capable of reaching deep brain areas with high spatial resolution [4–6]. Still, while TUS is a promising neuromodulation technique, many challenges remain in understanding its underlying mechanisms, for example how it translates into either stimulation or inhibition of neural activity [6–9]. Challenges in advancing the understanding of TUS effects include: (i) disentangling the spatially widespread changes generated by stimulus-induced plasticity, (ii) moving from population-level to individual-level descriptions, which are essential to designing personalized therapies, and (iii) predicting TUS effects via biologically realistic mechanisms. Here, we address these challenges by joining high-order interdependencies [10], communication models [11], and whole-brain modeling [12,13]. Our aim is to identify robust informational markers to assess the alterations in brain function induced by stimulation, and to uncover their underlying biophysical mechanisms.

There are multiple ongoing research efforts trying to unravel the widespread changes generated by TUS. At the cellular level, the interaction of acoustic waves with the neuronal membrane in TUS has been investigated in terms of the activation of mechanosensitive ion channels or astrocytic TRPA1 [14–16], GABA inhibition [17] or cavitation [18,19]. These mechanisms are related to synaptic plasticity processes, such as Long-Term Potentiation (LTP) and Long-Term Depression (LTD), by modulating neuronal excitability and neurotransmitter release [20]. At a global level, studies on functional connectivity have shown the impact of stimulus-induced plasticity at the population-level, revealing both increases and decreases in connectivity [21–24]. Additionally, high-order informational dependencies (HOI) have been used to characterize how TUS reorganizes the brain at the individual-level [25]. The core advancement of these methods with respect to traditional functional connectivity lies in their capacity to encode redundancy and synergy among signals [26–28]. For a simple example of the additional information encoded by these quantities, consider cooking. Individual ingredients might not provide a notable impact on texture, smell, and taste. However, when combined in a recipe, they create a different and –hopefully– memorable experience by working synergistically. Conversely, using multiple ingredients with similar texture or flavor would result redundant, because the same information is present among multiple ingredients.

After gaining insight into the functional changes induced by stimulation, we can use this knowledge to develop models that explain the plasticity-driven effects. This requires two elements: communication models, and whole-brain models. The former, communication models, are needed to describe how stimuli propagate across anatomically connected regions [11, 29–31]. In this context, navigation frameworks, such as shortest path length, have been widely applied to characterize neural communication [32–34]. However, diffusion models have recently demonstrated greater predictive power than efficiency-based approaches in explaining functional effects [11,35], a notable example of this being recent results on the propagation of focal electrical stimulation in intracranial EEG recordings of drug-resistant epilepsy participants,[36]. Whole-brain models involved instead the integration of structural connectivity and neuronal dynamics [13,37–40] to enable the testing of mechanistic hypotheses, including biophysically inspired ones [12,41].

Here, by combining these elements, we aim to elucidate: (i) to what extent high-order functional interactions to localize TUS-induced spatial effects; (ii) how widespread is the propagation of a stimulus across the brain when its magnitude increases; and (iii) which network communication model of the *TUS-induced plasticity* better explains mechanistically the *functional changes* induced by the stimulation. To address these questions, we analyze fMRI data of human subjects stimulated at two different targets: the right inferior frontal cortex and the right thalamus. We show that the TUS of each induces a specific signature of spatially widespread redundant and synergistic changes. Specifically, for the inferior frontal cortex stimulation (TUS-IFC), we observe effects in the frontal and basal ganglia areas, while for the thalamic stimulation (TUS-Thal), effects are prominent in the cingulate, temporal, and basal ganglia regions. Additionally, we find that communication models based on network communicability and distance are more reliable predictors of high-order functional changes than other communication models for both stimuli. Lastly, using the two most informative communication models for the plasticity, we develop a whole-brain model, reproducing the spreading of the stimulation throughout the brain as the stimulus intensity increases.

Results

We analyzed changes in redundancy and synergy in fMRI data following TUS. The participants underwent an initial fMRI session lasting approximately 14 minutes without stimulation (control, N = 22). On a separate day, they received 80 seconds of TUS, with participants receiving stimulation targeted at either the right inferior frontal cortex (TUS-IFC, N = 11) or the right thalamus (TUS-Thal, N = 11) (Fig 1A), followed by an fMRI scan lasting around 42 minutes.

We calculated redundancy and synergy (Fig 1B) for each pair of time series using the Integrated Information Decomposition method [28]. This approach decomposes the information of two variables measured at two consecutive time points into redundant, synergistic, and unique components that characterize specific dynamical patterns. Following previous work [44], our analysis focused only on the redundant and synergistic interactions, neglecting the unique information component (see *Methods* for further details). To assess the relative relevance of every brain region in synergistic or redundant interactions, we ranked regions by their redundancy-strength (median-redundancy-rank) and synergy-strength (median-synergy-rank).

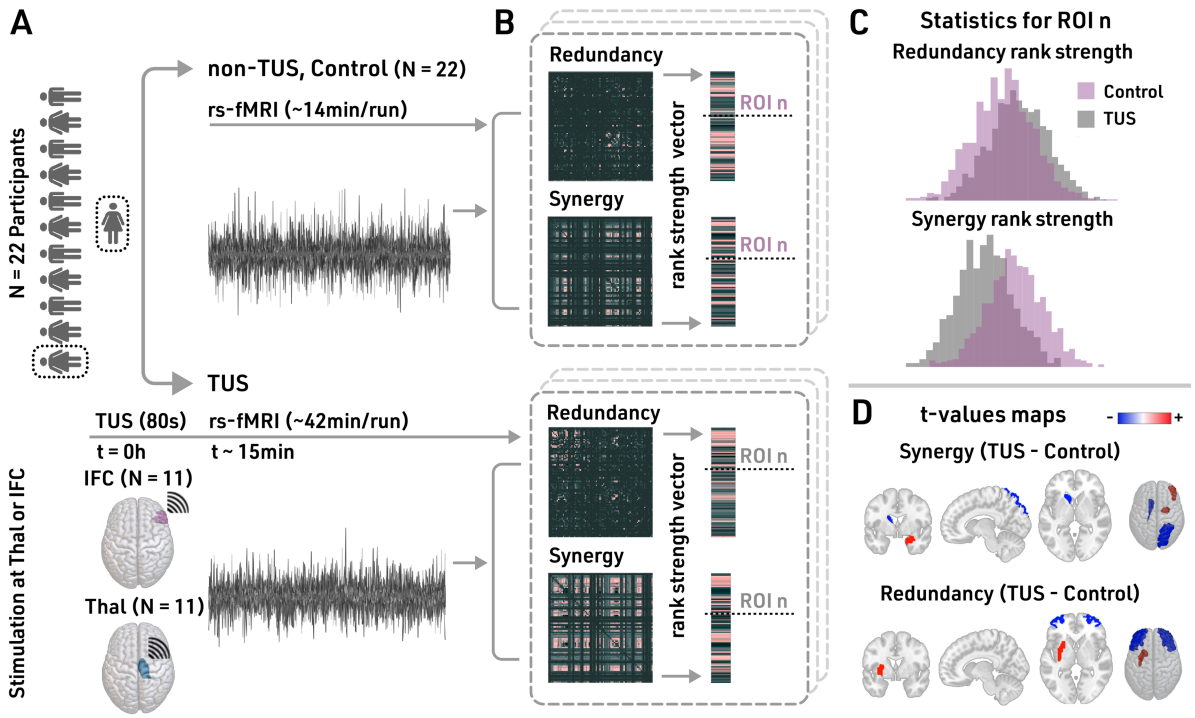

Fig 1. Methodology and absolute changes in redundancy and synergy after TUS. A. Twenty two subjects participated in the experiment, $N = 22$ controls (non-TUS), $N = 11$ IFC-TUS, and $N = 11$ Thal-TUS. **B.** We quantified the redundancy and synergy matrices, computing their median vector across rows and their ranked version, named median-redundancy-rank or median-synergy-rank. **C.** For each ROI, we compared each median-HOI-rank/absolute distribution (dotted line in **B**) between the control and TUS. **D.** We reported the t-values for the absolute changes, representing a shift to an increase (red) or decrease (blue) HOI interactions.

https://doi.org/10.1371/journal.pcbi.1013514.g001

Transcranial ultrasound stimulation alters HOI, revealing spatial localization

To observe local functional changes due to stimulation, we compared the distributions of the redundancy (median-redundancy-rank) and synergy (median-synergy-rank) (Fig 1B) between the control group (non-TUS) and each TUS condition for each brain area (Fig 1C–1D).

For TUS-IFC, we find alterations in the redundancy in frontal regions (parsorbitalis, right rostral middle frontal, right caudal middle frontal, and right paracentral), and basal ganglia areas (accumbens and caudate) (Fig 2A, top row). Statistics (t-values and p-values) for these findings are reported in S1 Table. Results also show changes in synergy at frontal (rostral middle frontal), parietal (supramarginal), temporal (temporal pole, entorhinal), and basal ganglia regions (putamen) (see S1 Table) (Fig 2A, bottom row).

In contrast, after TUS-Thal, the redundancy (Fig 2B, top row) changed at frontal (parstriangularis, lateral orbitofrontal), temporal (superior temporal, middle temporal), basal ganglia (accumbens), cingulate (posterior cingulate), and occipital (lateral occipital). The synergy showed differences at the cingulate (rostral anterior cingulate), temporal (entorhinal), and basal ganglia areas (pallidum and thalamus). We report the statistics (t-values and p-values) in S1 Table.

In conclusion, the functional effects induced by TUS vary significantly depending on the stimulation target, leading to distinct spatial patterns. Overall, after TUS-IFC redundancy and

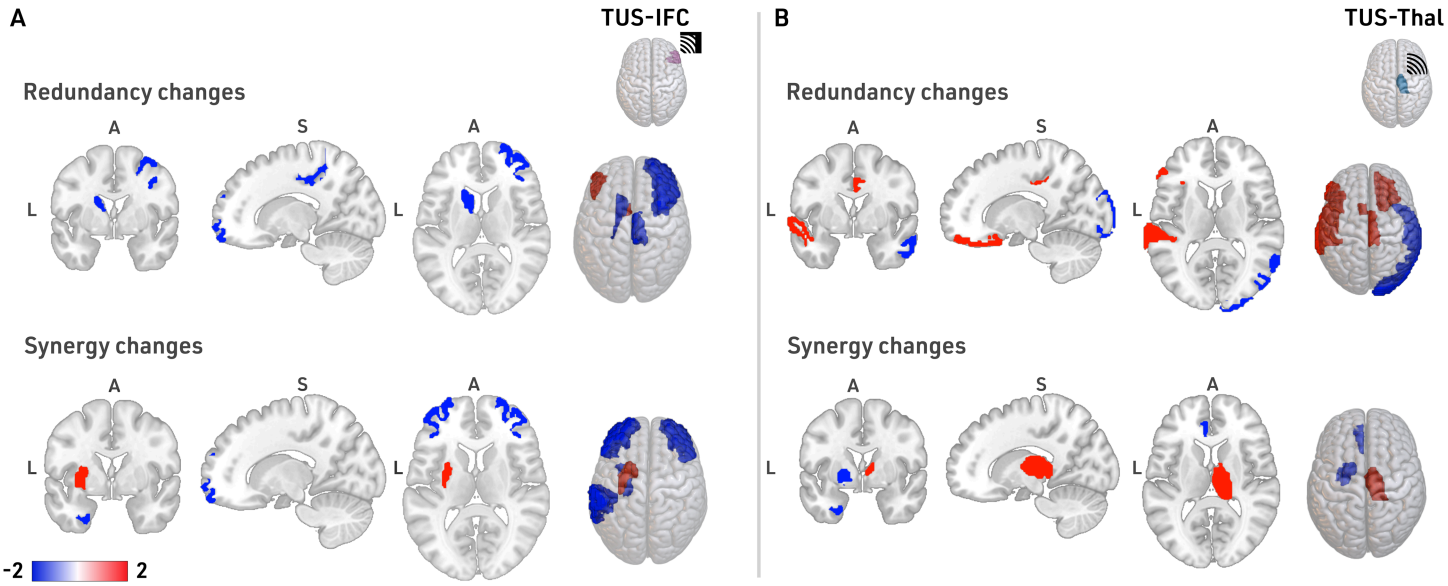

Fig 2. Relative changes in redundancy and synergy after TUS. A. Top row: median-redundancy-rank distribution changes after the TUS-IFC. Bottom row: Median-synergy-rank distribution changes after the TUS-IFC. The blue represents a region decreasing the HOI after TUS, wheres the red color describes the increase. **B.** Similar to A, when the target is the thalamus (TUS-Thal). We reported the t-values corrected by a $N = 1000$ permutation test in all the comparisons.

https://doi.org/10.1371/journal.pcbi.1013514.g002

synergy show changes in the frontal and basal ganglia areas, with synergy additionally extending into the temporal and parietal lobes. When focusing on the frontal areas, the redundancy presented lateralized changes, mainly decreasing in the right hemisphere, particularly in the rostral and caudal middle frontal regions and the paracentral lobule. In contrast, after TUS-Thal, both quantities presented spatially widespread functional changes in the basal ganglia, temporal, and cingulate regions, extending redundancy into the frontal and occipital lobes. Interestingly, only the synergy showed an increase in the right thalamus, which was the targeted area for stimulation.

Distance and communicability predict changes in HOI

After characterizing the local effects induced by TUS, we aim to determine which communication models best explain the global HOI effects produced by the stimulation. To approach this, we examine the associations of changes in redundancy and synergy with various models of stimulus propagation, based either on efficient navigation or on diffusion. In particular, following previous work (see [36] and *Methods* for further details), we adopt streamline length (distance) and shortest path efficiency (SPE) as proxies for efficiency, and search information (SI) and communicability (CMY) as a proxy for diffusion. To compute the associations between HOI changes and these models, we created eight "representative" vectors: one for each of the four connectivity models (distance, SPE, SI, CMY), and four representing redundancy and synergy changes for the two targets (TUS-IFC or TUS-Thal minus control), respectively. We describe these vectors as *representative*, because the models were computed using group-averaged properties (more specifically, average anatomical or functional matrices; see Methods for details), rather than individual measurements. Then, for each target, we correlated the vectors corresponding to the four models with those representing the changes in redundancy and synergy for that target, where by changes here we refer to the difference

between the measurements after stimulation and those in the control condition (e.g. TUS-IFC minus control).

Surprisingly, we found two opposing patterns (Fig 3). For TUS-IFC, redundancy alterations are negatively correlated with both network communicability ($r = -0.381$, $p<0.001$) and distance ($r = -0.569$, $p<0.001$), while synergy alterations are not significantly correlated with any of the two (Fig 3A). For TUS-Thal, synergy alterations are positively correlated with both network communicability ($r = 0.353$, $p = 0.001$) and distance ($r = 0.439$, $p<0.001$), while redundancy ones are not correlated with any of the two (Fig 3B). All other communication models do not give any significant result, with exception of a negative correlation of synergy with shortest path efficiency for TUS-Thal ($r = -0.325$, $p = 0.003$. S1 Fig).

In both cases, the largest changes in absolute value for both redundancy and synergy after stimulation were associated with longer distances and with regions (see Fig 3A and 3B, top row). However, in this case too, the effects are opposing: for TUS-IFC we observe an overall decrease of redundancy with distance from the stimulation (Fig 3A, top row); for TUS-Thal instead we find an overall increase in synergy with distance from the stimulation. Together these findings suggest the presence of a strong network effect in the TUS-induced plasticity, possibly mediated by the multiplicity of propagation paths between regions [55].

Whole-brain model informed by distance or communicability heterogeneity explains changes in HOI

To test the hypothesis of a mechanistic link between the observed global effects of TUS on HOI and communication models encoding different notions of connectivity, we propose a whole-brain model which explicitly includes communicability and distance as mechanisms affecting redundancy and synergy. Specifically, we used a Hopf model of neural oscillators, in which the local dynamics of each node was simulated using the Stuart-Landau oscillator. For

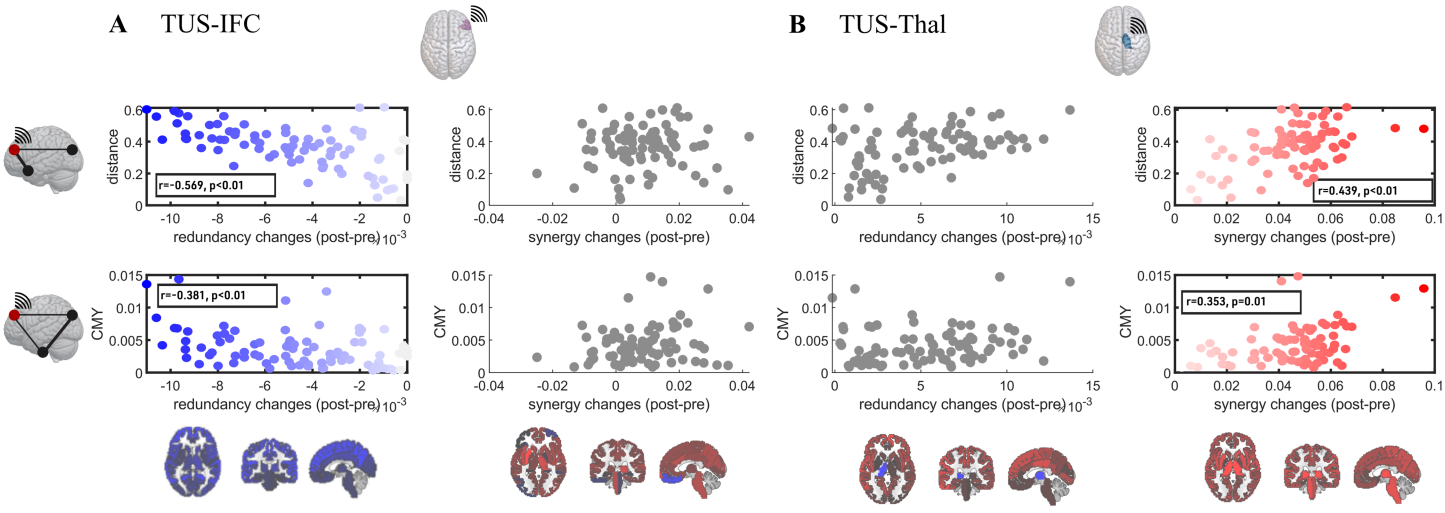

Fig 3. Whole-brain associations between structural models and observed changes in TUS. For TUS-IFC **A.** and TUS-Thal **B.**, we computed the models and changes in HOI (after minus before) over a representative matrix (redundancy, synergy, distance, and the communicability, CMY) averaged across all participants. Within each subpanel, each row corresponds to a structural model (distance, top row; communicability model, CMY, bottom row), while each column corresponds to changes in informational quantities (redundancy, left column; synergy, left right column). The darker boxes represent the p-values lower than 0.05 after the Bonferroni correction, with the blue dots representing the redundant and red dots the synergistic changes. The grey colour dots represent the non-significant associations. For the other two models, see S1 Fig.

https://doi.org/10.1371/journal.pcbi.1013514.g003

positive bifurcation parameter ($a>0$), the model enters a limit cycle, and the system exhibits sustained oscillations. For negative bifurcation parameter ($a<0$), the model has a stable fixed point, and thus the system will be dominated by noise. Finally, near the bifurcation point ($a = 0$), noise-driven and sustained oscillations coexist in time (Fig 4A).

To include different notions of TUS propagation, we informed the model using communicability or distance (denoted as β^n), and a stimulation strength (denoted by $\alpha\ \beta_n^s$) to quantify the changes in the TUS (Fig 4B). Our approach involved a two-step fitting process as outlined in previous literature [53]. First, we performed a homogeneous fitting to determine the optimal global coupling (G). Then, we conducted a heterogeneous fitting to obtain the "bias" and "scale" parameters (Fig 4B) to fit the control condition (see S2 Fig). In both cases, the goal was to achieve model simulations that reproduce as closely as possible the functional connectivity and mean brain synchrony (computed as the average Kuramoto order parameter, KOP) measured in data. Finally, after fitting the control condition, we simulated the effects of stimulation over a range of perturbation intensities (described by the parameter α).

Using the calibrated models, we examined the similarity between the empirical and simulated HOI effects of TUS, revealing three key findings. First, negative α values lead to better performance regardless of the target (Fig 4C, α in the x-axis). Specifically, when α is negative, it results in larger positive correlations between the simulated and observed HOI values, whereas positive α values produced smaller, anti-correlated values. This suggests that the stimulation is likely disrupting the excitatory/inhibitory balance by increasing inhibition (noise), rather than by enhancing excitation (synchronization). Moreover, when α increased, the time series became progressively more synchronized, with the thalamus stimulation leading to faster system synchronization (see S3 Fig). Second, for both targets and negative α, redundancy changes were best reproduced by the distance-based model, while synergy changes were more accurately captured by the communicability model. Third, moving from strongly negative to strongly positive α, we consistently observed a local-to-global transition characterized by three main regimes: (i) only localized effects on a handful of regions for $\alpha \ll 0$, (ii) an intermediate regime in which no region shows significant alterations in their synergy/redundancy behaviours for $\alpha \sim 0$ (Fig 4D, dashed red area), finally, (iii) global, delocalized effects across the whole brain for both redundancy and synergy for $\alpha \gg 0$. Notably, in the simulated TUS-IFC condition, in the localized regime ($\alpha \ll 0$), we recovered the redundancy alterations in the right IFC (Fig 4D, first panel, blue triangle) but not synergistic ones (Fig 4D, second panel, white triangle). Conversely, for the TUS-Thal condition, only the synergistic alterations in the right thalamus were reproduced (Fig 4D, fourth panel, red triangle).

Discussion

Our results revealed distinct patterns of functional reorganization following TUS, depending on the target. We obtained these findings combining three innovations: (i) the application of HOI to localize spatial effects induced by TUS in humans, extending previous studies in macaque data [21,22,25], (ii) the use of communication models as mechanisms to predict the functional plasticity-driven impact of TUS, and (iii) the development of a model to explain the mechanism of propagation of the effects of TUS when the stimulation intensity increases. We found that, for TUS-IFC, HOIs exhibited changes in frontal and basal ganglia areas, with the redundancy decreasing in the right frontal hemisphere, whereas, for TUS-Thal, changes were localized in the cingulate, temporal, and basal ganglia areas, with the synergy increasing in the stimulated right thalamus. Although the TUS protocol is designed to modulate neuronal activity by either increasing or decreasing it, studies have observed both increased and decreased functional connectivity [21–24], as well as higher-order interactions [25] in

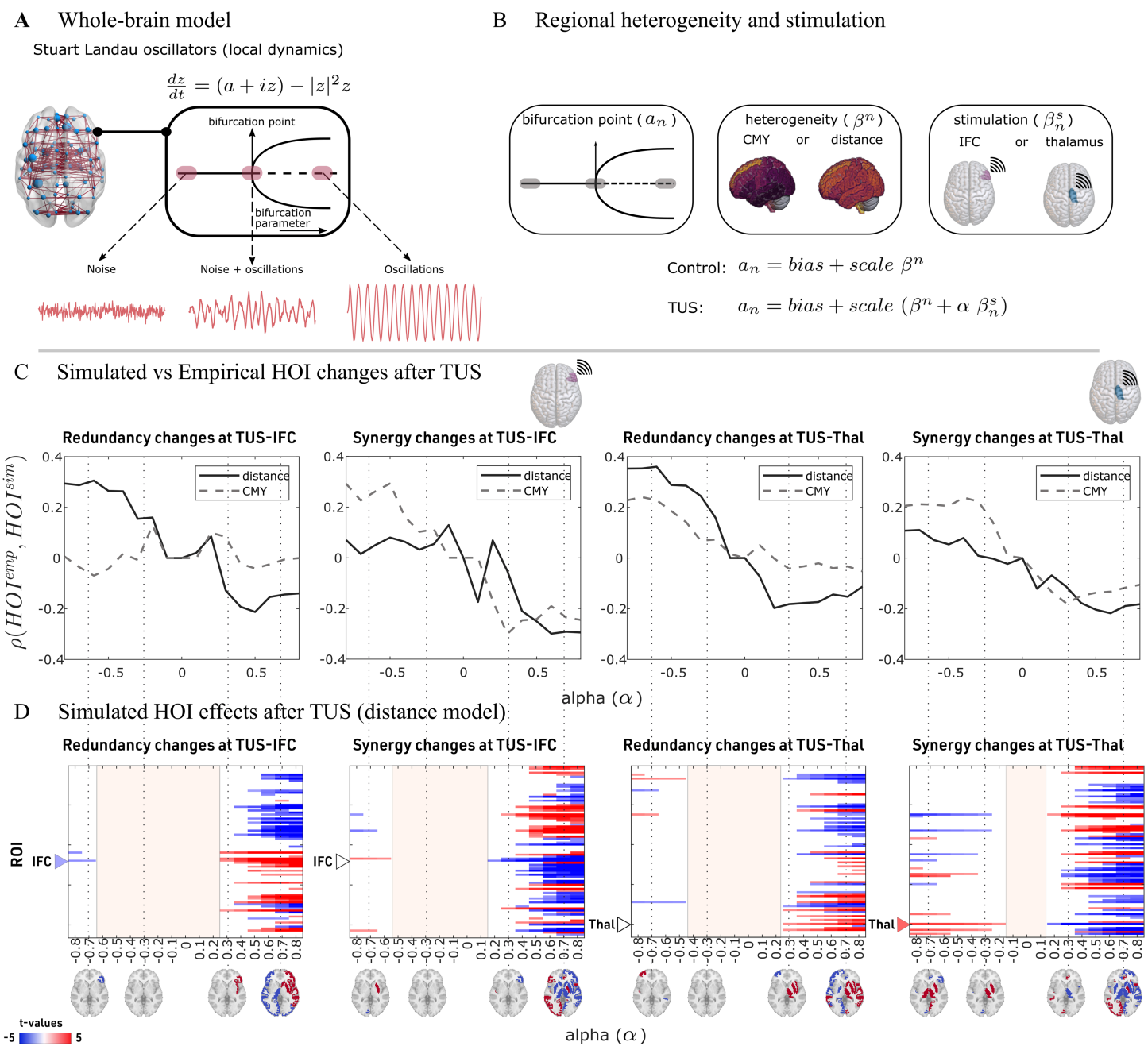

Fig 4. Whole-brain modeling predicts the propagation of TUS-induced plasticity from local to global scales. A. The local dynamics of each node were simulated using the Stuart-Landau oscillator, which, depending on the bifurcation parameter (a), can exhibit sustained oscillators (a>0), noise (a<0) or coexistence of noise-driven and sustained oscillations (a = 0). **B.** We inform heterogeneous models with communication models based on communicability (CMY) or distance (denoted as β^n), and a stimulation modulated by the parameter α (denoted by $\alpha\ \beta_n^s$) for each target. **C.** Redundancy and synergy fitting between the empirical and simulated data: The x-axis corresponds to different simulated intensities in the model (alpha), while the y-axis to the Spearman correlation between the empirical and simulated statistical differences (all the t-values in TUS minus control). Each column corresponds to the changes in redundancy and synergy for the two targets. Results for the model based on distance are shown with a solid line, those for the one based on the communicability model with a dashed line. **D.** Corrected t-values in the simulated data (TUS minus control) for the distance-based model (for the communicability model, see S4 Fig). The columns are consistent with panel **C**. The brain plots illustrate the HOI changes, displaying significant t-values corrected using a permutation test with N = 1000 iterations. Colors indicate negative/positive changes with respect to no stimulation. Coloured triangles represent the stimulated target with significant t-values at negative alpha.

https://doi.org/10.1371/journal.pcbi.1013514.g004

macaques following TUS. This variability may arise from a combination of LTP or LTD-like plasticity effects, resulting in heterogeneous outcomes [21,22,56].

We reported two possible mechanisms for plasticity induced by the stimulation to predict the functional changes after TUS. The global functional changes produced by TUS were associated with distance and communicability regardless of the targeted area. In turn, models based on distance and communicability outperformed models based on shortest path efficiency and search information. Altogether, our findings align with results from drug-resistant epilepsy participants [36], in reported communicability and search information —both diffusion processes— were found to be the best predictors for the propagation of focal electrical stimulation. Our results also align with previous research predicting functional connectivity patterns based on network communication, in which diffusion models were shown to outperform models based on shortest path length [35]. We believe that these findings provide valuable insights for modeling the effects of various types of stimulation and suggest potential avenues for further research and clinical applications [11].

We developed a whole-brain model explaining how the effects of TUS spread spatially throughout the brain as the stimulation intensity increases. In particular, depending on the intensity, the effects transitioned from a localized to a global regime, opening new paths for the exploration and prediction of changes in brain function. We also found that larger stimulation intensities led to quicker synchronization in the thalamus compared to the IFC. This can be explained by the thalamus's more central role in system integration [57–60], which would increase its capacity to promote more synchronized interactions. Moreover, we implemented two possible mechanisms of TUS propagation, one based on distance and one broadcasting process that allowed us to test the plasticity-driven changes in some brain areas for different intensities. Similar to adjusting the bifurcation parameter in the Hopf model, biophysically-inspired models have shown a transition from noisy oscillations to sustained oscillations when the excitatory/inhibitory (E/I) balance is disrupted through increased inhibition or excitation, respectively [49–52]. Furthermore, bifurcation diagrams establish a connection between realistic models, such as the Wilson-Cowan model, and the bifurcation parameter in the Hopf model. In the Wilson-Cowan model, shifting the E/I balance toward excitation leads to sustained oscillations, while moving it toward inhibition results in damped activity [61]. In our findings, both models indicated that the stimulus is more likely to induce noise in the system rather than pure synchrony. This suggests that the stimulus tends to disrupt the E/I balance by enhancing inhibition rather than excitation. We stress that –although the mechanisms of TUS or the plasticity-induced chances are still a matter of debate [14–19]– which mechanism leads to either inhibitory or excitatory outcomes is even less understood [8,17,19,62]. The theta-burst TUS protocol used in this study has been associated with an increase and decrease in neural activity [63], and our model could help clarify whether ultrasonic neuromodulation produces excitatory or inhibitory effects. The whole-brain models have been used on perturbations and psychiatric or neurological conditions, enabling to test mechanisms that can be used for predicting the outcomes of real experimental settings [37–40,64].

Higher-order interactions have gained prominence in clinical applications for characterizing and predicting healthy aging [39,65,66], early development [67], neurological conditions [68,69], and their associations with cognition [44] and consciousness [70]. Recently, HOI has been applied to transcranial ultrasound stimulation (TUS) in macaques, revealing different topological reorganizations depending on the stimulation target [25]. Here, we extended this understanding to healthy humans, demonstrating that spatial differences in response to TUS also rely on the stimulation target.

Before concluding, it is important to acknowledge the limitations of this study. First, our experiment included 22 participants. Future studies should build on this by incorporating a larger sample size to enhance the robustness of the results. Second, the experimental protocol involves session-to-session variability, as the control and stimulation sessions are conducted on separate days. This may introduce additional variability in the estimation of HOI. Future studies employing online stimulation protocols could mitigate this issue by enabling recordings before, during, and after TUS within a single session. Third, we proposed a mechanism for modifying regional excitability. While the effects of perturbing only the stimulated target have been observed, this presents an exciting avenue for future research, such as further exploring the impact of stimulating both the target and adjacent areas. Finally, while we used the minimum mutual information (MMI) redundancy function, as supported by previous literature demonstrating its clinical relevance in cognition [44], similar outcomes might be attainable with other redundancy functions [71]. Exploring alternative definitions [72,73] could offer valuable opportunities for further investigation.

Materials and methods

Ethics statement

The study adhered to the ethical standards of the Helsinki Declaration of 1978, as revised in 2008, and received approval from the University of Nottingham Faculty of Psychology Ethics Committee (reference: F1298R, 28/03/2022). After providing detailed information and answering all questions, participants provided written consent.

Participants

Twenty-two healthy, right-handed volunteers participated in this study. None had a history of neurological or psychiatric disorders (except for cases of depression considered remitted for at least one year) and were not taking any medications. The additional exclusion criteria included close relatives with a history of seizures, a predisposition for syncope, excessive hair that could interfere with transducer coupling, current or planned pregnancy, implanted metallic devices, skin diseases, claustrophobia, or anxiety related to MRI, and tattoos near the head. Participants were instructed to avoid recreational drugs for 48 hours before their visits and to limit alcohol consumption to no more than four units within the preceding 24 hours. The study was conducted in two sessions. During the first session, participants underwent a 45-minute MRI scan, which included a 14-minute resting-state fMRI sequence. They returned for a second session on a different day, scheduled at the same time of day as their initial visit (time difference: 55.4±40.1 minutes for the IFC group vs. 69.5±48.9 minutes for the thalamus group; p=0.469). Participants were pseudo-randomly assigned to one of two groups, ensuring an equal distribution of sexes, based on the TUS brain target: either the right inferior frontal cortex or the right thalamus. Immediately following stimulation, participants underwent another 45-minute MRI session (delay between TUS and rs-fMRI: 15±2.16 minutes for the IFC group vs. 15.4±1.37 minutes for the thalamus group; p=0.95), which included a 42-minute rs-fMRI sequence.

Detailed information on data acquisition and preprocessing is available in S1 Text.

Partial Information Decomposition (PID)

Consider three random variables: two source variables X^i and X^j, and a target variable Y. The Partial Information Decomposition (PID) [42] decomposes the total information provided by

X^i and X^j about Y, given by Shannon's mutual information $I(X^*; Y)$, as follows:

$$\begin{aligned} I(X^i, X^j; Y) = \quad & \mathrm{Red}(X^i, X^j; Y) + \mathrm{Syn}(X^i, X^j; Y) \\ & + \mathrm{Un}(X^i; Y|X^j) + \mathrm{Un}(X^j; Y|X^i), \end{aligned} \tag{1}$$

where $\mathrm{Red}(X^i, X^j; Y)$ represents the information provided by X^i and X^j about Y (redundancy), $\mathrm{Syn}(X^i, X^j; Y)$ denotes the information provided jointly by X^i and X^j about Y (synergy), $\mathrm{Un}(X^i; Y|X^j)$ is the unique information provided by X^i about Y, and $\mathrm{Un}(X^j; Y|X^i)$ is the information that is provided only by X^j about Y. The four terms of this decomposition are naturally structured into a lattice with nodes $\mathcal{A} = \{\{12\}, \{1\}, \{2\}, \{1\}\{2\}\}$, corresponding to the synergistic, unique in source one, unique in source two, and redundant information, respectively. To compute these terms, we followed the minimum mutual information (MMI) PID decomposition for Gaussian systems [43], where the redundancy is computed as the minimum information between each source and the target, and the synergy refers to the additional information provided by the weaker source when the stronger source is known.

Integrated information decomposition (ΦID). Consider the stochastic process of two random variables $X_t = \{X_t^i, X_t^j\}$ and denote the two variables in a current state t, by X_t^i and X_t^j, and the same two variables in a past state $t - \tau$, by $X_{t-\tau}^i$, and , $X_{t-\tau}^j$. The integrated information decomposition (ΦID) is the forward and backward decomposition of $I(X_{t-\tau}^i, X_{t-\tau}^j; X_t^i, X_t^j)$, called the time delay mutual information, in redundant, synergistic and unique information [28]. The ΦID can be represented by the forward and backward interactions of the product $\mathcal{A} \times \mathcal{A}$, resulting in 16 distinct atoms: synergy to synergy, redundancy to redundancy, unique in source one to unique in source two (and backward), and redundancy to synergy, among others. Following previous work [44], our analyses focus on two specific atoms quantifying the temporal persistence of redundancy and synergy: persistent redundancy (redundancy that remains redundancy) and persistent synergy (synergy that remains synergy).

Note that while some approaches to assessing higher-order interactions involve three or more time series, we employed the "higher-order" concept here as we analyzed four random variables $\{X_{t-\tau}^i, X_{t-\tau}^j; X_t^i, X_t^j\}$, where (X^i, X^j) represent the two variables at the current state t, along with $(X_{t-\tau}^i, X_{t-\tau}^j)$ being their states at $t - \tau$.

Synergy and redundancy rank framework. The ΦID was computed for all combinations of pairwise BOLD time series X_t^i, X_t^j, where i and j represent two different brain regions, with $(i, j) \in 1, \ldots, 84$. This resulted in two symmetrical matrices capturing redundancy and synergy. We then calculated the median of each matrix to obtain two strength vectors (each 1x84) representing redundancy and synergy. Additionally, we derived rank strength vectors for both redundancy and synergy (each 1x84), ranking each region by its strength. Finally, we compared the absolute or rank strength values between the TUS (IFC-TUS or Thal-TUS) and the Control vector.

Distance and communication models

$D \in \mathbb{R}^{84\times84}$ denotes the distance with D_{ij} being the average streamline length between two regions i and j, computed per subject. As a representative value of *distance*, we used an average across subjects normalized by the maximum ($distance = \overline{D}/max(\overline{D})$). Similarly, $M \in \mathbb{R}^{84\times84}$ denotes the structural connectivity, where M_{ij} is defined as the average number of streamlines connecting two brain regions i and j. We computed an average across subjects as the representative structural connectivity, denoted by $\overline{M}$, likewise normalized with real values between zero and one. Then, we computed the matrix of lengths $L = 1/\overline{M}$, with L_{ij} the cost of communication between the regions i and j.

The *Shortest Path efficiency* is denoted by *SPE*, where (SPE_{ij}) is computed as the inverse of the shortest path or geodesic connecting two nodes *i* and *j*. Given the sequence of regions $\{i, u, \ldots, v, j\}$, such that $\Lambda^*_{ij} = L_{iu} + \cdots + L_{vj}$ is the minimum transmission cost between *i* and *j*, then $SPE_{ij} = 1/\Lambda^*_{ij}$ [45].

The *Search Information* is denoted by *SI* and quantifies the amount of information to bias a random walk into the shortest path $\{i, u, \ldots, v, j\}$. The transition probability of traveling from *i* to *j* is computed as $T_{ij} = \overline{M}_{ij} / \sum_{k=1}^{84} \overline{M}_{ik}$. Therefore, the probability of a random walk to travel from *i* to *j* via the shortest path is $\Pi_{ij} = T_{iu} \times \cdots \times T_{vj}$. Finally, the search information (SI_{ij}) is computed as $SI_{ij} = -\log_2(\Pi_{ij})$ [35].

The *Communicability*, denoted by *CMY*, is a broadcasting process quantifying the redundant walks connecting two regions while penalizing the longer paths. Therefore, $CMY_{ij} = \sum_{n=0}^{\infty} W'^{n}_{ij}/n! = e^{W'_{ij}}$, where $W'_{ij} = W_{ij}/(\sqrt{s_i}\sqrt{s_j})$, and $s_i = \sum_{n=1}^{84} s_n$ is the strength of region *i* [46, 47].

Whole-brain model

We simulated the brain activity using a supercritical Hopf bifurcation model (Stuart-Landau oscillators) [37,48]. The following ordinary differential equations [3] define the dynamic for each node *i*:

$$\begin{aligned} \frac{dx_i(t)}{dt} = {} & a_i x_i(t) - \left[x_i^2(t) - y_i^2(t)\right] x_i(t) \\ & - w_i y_i(t) + \gamma \eta_i(t), \\ \frac{dy_i(t)}{dt} = {} & a_i y_i(t) - \left[x_i^2(t) - y_i^2(t)\right] y_i(t) \\ & + w_i x_i(t) + \gamma \eta_i(t). \end{aligned} \tag{2}$$

Where $y(t)$ corresponds to the imaginary component, and the real component of the time series, $x(t)$, simulated the BOLD-like signals. We set the oscillation frequency $f_i = 0.05$ Hz ($w_i = 0.05 \times 2 \times \pi$) for overall nodes. When the bifurcation parameter *a* is positive ($a > 0$), the system exhibits a limit cycle, leading to sustained oscillations. If ($a < 0$), the system has a stable fixed point and is dominated by noise. Near the bifurcation point ($a = 0$), both noise-driven and sustained oscillations coexist over time. We used 84 nodes, parcellated using the Desikan-Killiany atlas (See S2 and S3 Tables for details), including subcortical areas and structural connectivity matrices $M \in \mathbb{R}^{84\times84}$ (19 matrices. As described in S1 Text, three images were excluded due to excessive motion). The brain areas are coupled with the structural connectivity *M*, $G = 0.16$ represents the global coupling (S2 Fig), and $\eta_i(t)$, with $\gamma = 0.02$ the standard deviation, the external Gaussian noise [3].

$$\begin{aligned} \frac{dx_i(t)}{dt} = {} & a_i x_i(t) - \left[x_i^2(t) - y_i^2(t)\right] x_i(t) - w_i y_i(t) \\ & + G \sum_{j=1}^{n} M_{ij} \left(x_j(t) - x_i(t)\right) + \gamma \eta_i(t), \\ \frac{dy_i(t)}{dt} = {} & a_i y_i(t) - \left[x_i^2(t) - y_i^2(t)\right] y_i(t) + w_i x_i(t) \\ & + G \sum_{j=1}^{n} M_{ij} \left(y_j(t) - y_i(t)\right) + \gamma \eta_i(t). \end{aligned} \tag{3}$$

We proposed modifying the bifurcation parameter as a proxy of modulate neuronal activity. Biophysical-inspired models have revealed a switch from noisy oscillations to sustained

oscillations (limit cycles) when disrupting the excitation/inhibition balance through excitation [49–52], analogous to increasing the bifurcation parameter in the Hopf model. Following previous literature, we incorporated heterogeneity in our model [53].

Control and TUS model. We simulated the control condition using the Hofp model with $a_i = bias + scale\,\beta^i$, where β is the heterogeneous vector of distances or communicability. The parameters *scale* and *bias* were fitted as $(bias, scale) = (-0.17, 0.24)$ in the distance model and $(bias, scale) = (-0.08, 0.21)$ in communicability (see S2 Fig). Additionally, for TUS, $a_i = bias + scale\,(\beta_i + \alpha\,\beta_i^s)$, where $\beta_i^s = 1$ if s is the stimulated target and zero in other case.

We ran 1100s simulations with an integration step of 0.1s in the Euler-Maruyama integration scheme for each subject (19 structural connectivity matrices). The simulated time series were band-pass filtered between 0.001 and 0.01 Hz and removed the first and last 100s, resulting in 15-minute simulations.

Statistical analysis

This study compared the redundancy and synergy of each control (non-TUS) versus each TUS experiment (IFC-TUS or Thal-TUS) using a t-stat (TUS minus control). We performed a 1.000 permutation two-samples t-test analysis per region in the empirical data and the simulations to find the statistically significant differences. Bonferroni corrected the correlations between redundancy and synergy changes with the communication models.

Supporting information

S1 Fig. Whole-brain associations between structural models and observed changes in TUS. For TUS-IFC **A.** and TUS-Thal **B.** Within each subpanel, the rows correspond to the search information (SI) and short path efficiency (SPE) models, while each column to changes in informational quantities (redundancy, left column; synergy, left right column). The darker boxes represent the p-values lower than 0.05 after a Bonferroni correction.
(EPS)

S2 Fig. Whole-brain fitting. A. Homogeneous model for the control condition (non-TUS) **B.** Heterogeneous distance model for non-TUS. **C.** Heterogeneous communicability model for non-TUS. The first column corresponds to the differences in synchrony (measured as the mean of the Kuramoto order parameter) between the empirical and simulated data. The second column is the correlation between the functional connectivities between the simulations and the empirical data, and the third column is the multiplication of the two former columns.
(EPS)

S3 Fig. Modulation of synchrony by stimulation intensity. Synchrony differences (mean(KOP)) between empirical data and the target at various intensities, modulated by α, for each model (distance in solid line, and communicability in dashed line).
(EPS)

S4 Fig. Simulated HOI effects after TUS. Similar to Fig 4D, for the communicability model.
(EPS)

S1 Table. Relative redundancy and synergy changes after TUS.
(XLSX)

S2 Table. Desikan-Killiany atlas, including subcortical areas: right hemisphere.
(XLSX)

S3 Table. Desikan-Killiany atlas, including subcortical areas: left hemisphere.
(XLSX)

S1 Text. Data acquisition, FUS protocols, and image preprocessing.
(DOCX)

Author contributions

Conceptualization: Marcus Kaiser, Giovanni Petri.

Data curation: Marilyn Gatica, Cyril Atkinson-Clement.

Formal analysis: Marilyn Gatica.

Funding acquisition: Marcus Kaiser.

Investigation: Marilyn Gatica.

Methodology: Marilyn Gatica, Pedro A. M. Mediano, Enzo Tagliazucchi, Fernando E. Rosas, Giovanni Petri.

Software: Marilyn Gatica, Carlos Coronel-Oliveros.

Supervision: Marcus Kaiser, Giovanni Petri.

Visualization: Marilyn Gatica.

Writing – original draft: Marilyn Gatica, Giovanni Petri.

Writing – review & editing: Cyril Atkinson-Clement, Carlos Coronel-Oliveros, Mohammad Alkhawashki, Pedro A. M. Mediano, Enzo Tagliazucchi, Fernando E. Rosas, Marcus Kaiser.

References

1. Legon W, Sato TF, Opitz A, Mueller J, Barbour A, Williams A, et al. Transcranial focused ultrasound modulates the activity of primary somatosensory cortex in humans. Nat Neurosci. 2014;17(2):322–9. https://doi.org/10.1038/nn.3620 PMID: 24413698
2. Polanía R, Nitsche MA, Ruff CC. Studying and modifying brain function with non-invasive brain stimulation. Nat Neurosci. 2018;21(2):174–87. https://doi.org/10.1038/s41593-017-0054-4 PMID: 29311747
3. Berlim MT, Eynde FVD, Daskalakis ZJ. Clinically meaningful efficacy and acceptability of low-frequency repetitive transcranial magnetic stimulation (rTMS) for treating primary major depression: a meta-analysis of randomized, double-blind and sham-controlled trials. 2013.
4. Tufail Y, Yoshihiro A, Pati S, Li MM, Tyler WJ. Ultrasonic neuromodulation by brain stimulation with transcranial ultrasound. Nat Protoc. 2011;6(9):1453–70. https://doi.org/10.1038/nprot.2011.371 PMID: 21886108
5. Legon W, Adams S, Bansal P, Patel PD, Hobbs L, Ai L, et al. A retrospective qualitative report of symptoms and safety from transcranial focused ultrasound for neuromodulation in humans. Sci Rep. 2020;10(1):5573. https://doi.org/10.1038/s41598-020-62265-8 PMID: 32221350
6. Darmani G, Bergmann TO, Pauly KB, Caskey CF, de Lecea L, Fomenko A. Non-invasive transcranial ultrasound stimulation for neuromodulation. 2022.
7. Sanguinetti JL, Hameroff S, Smith EE, Sato T, Daft CMW, Tyler WJ, et al. Transcranial focused ultrasound to the right prefrontal cortex improves mood and alters functional connectivity in humans. Front Hum Neurosci. 2020;14:52. https://doi.org/10.3389/fnhum.2020.00052 PMID: 32184714
8. Dell'Italia J, Sanguinetti JL, Monti MM, Bystritsky A, Reggente N. Current state of potential mechanisms supporting low intensity focused ultrasound for neuromodulation. 2022.
9. Sarica C, Nankoo JF, Fomenko A, Grippe TC, Yamamoto K, Samuel N. Human studies of transcranial ultrasound neuromodulation: a systematic review of effectiveness and safety. 2022.

10. Battiston F, Amico E, Barrat A, Bianconi G, Ferraz de Arruda G, Franceschiello B, et al. The physics of higher-order interactions in complex systems. Nat Phys. 2021;17(10):1093–8. https://doi.org/10.1038/s41567-021-01371-4
11. Seguin C, Sporns O, Zalesky A. Brain network communication: concepts, models and applications. Nat Rev Neurosci. 2023;24(9):557–74. https://doi.org/10.1038/s41583-023-00718-5 PMID: 37438433
12. Deco G, Tononi G, Boly M, Kringelbach ML. Rethinking segregation and integration: contributions of whole-brain modelling. Nat Rev Neurosci. 2015;16(7):430–9. https://doi.org/10.1038/nrn3963 PMID: 26081790
13. Lynn CW, Bassett DS. The physics of brain network structure, function and control. Nat Rev Phys. 2019;1(5):318–32. https://doi.org/10.1038/s42254-019-0040-8
14. Kubanek J, Shi J, Marsh J, Chen D, Deng C, Cui J. Ultrasound modulates ion channel currents. Sci Rep. 2016;6:24170. https://doi.org/10.1038/srep24170 PMID: 27112990
15. Kubanek J, Shukla P, Das A, Baccus SA, Goodman MB. Ultrasound elicits behavioral responses through mechanical effects on neurons and ion channels in a simple nervous system. J Neurosci. 2018;38(12):3081–91. https://doi.org/10.1523/JNEUROSCI.1458-17.2018 PMID: 29463641
16. Oh S-J, Lee JM, Kim H-B, Lee J, Han S, Bae JY, et al. Ultrasonic neuromodulation via astrocytic TRPA1. Curr Biol. 2019;29(20):3386-3401.e8. https://doi.org/10.1016/j.cub.2019.08.021 PMID: 31588000
17. Yaakub SN, White TA, Roberts J, Martin E, Verhagen L, Stagg CJ, et al. Transcranial focused ultrasound-mediated neurochemical and functional connectivity changes in deep cortical regions in humans. Nat Commun. 2023;14(1):5318. https://doi.org/10.1038/s41467-023-40998-0 PMID: 37658076
18. Plaksin M, Shoham S, Kimmel E. Intramembrane cavitation as a predictive bio-piezoelectric mechanism for ultrasonic brain stimulation. Phys Rev X. 2014;4(1). https://doi.org/10.1103/physrevx.4.011004
19. Plaksin M, Kimmel E, Shoham S. Cell-type-selective effects of intramembrane cavitation as a unifying theoretical framework for ultrasonic neuromodulation. eNeuro. 2016;3(3):ENEURO.0136-15.2016. https://doi.org/10.1523/ENEURO.0136-15.2016 PMID: 27390775
20. Citri A, Malenka RC. Synaptic plasticity: multiple forms, functions, and mechanisms. 2008.
21. Folloni D, Verhagen L, Mars RB, Fouragnan E, Constans C, Aubry J-F, et al. Manipulation of subcortical and deep cortical activity in the primate brain using transcranial focused ultrasound stimulation. Neuron. 2019;101(6):1109-1116.e5. https://doi.org/10.1016/j.neuron.2019.01.019 PMID: 30765166
22. Verhagen L, Cile Gallea C, Folloni D, Constans C, Jensen DE, Ahnine H, et al. Offline impact of transcranial focused ultrasound on cortical activation in primates. 2019.https://doi.org/10.7554/eLife.40541.001
23. Atkinson-Clement C, Alkhawashki M, Ross J, Gatica M, Zhang C, Sallet J, et al. Dynamical and individualised approach of transcranial ultrasound neuromodulation effects in non-human primates. Sci Rep. 2024;14(1):11916. https://doi.org/10.1038/s41598-024-62562-6 PMID: 38789473
24. Atkinson-Clement C, Alkhawashki M, Gatica M, Ross J, Kaiser M. Dynamic changes in human brain connectivity following ultrasound neuromodulation. Sci Rep. 2024;14(1):30025. https://doi.org/10.1038/s41598-024-81102-w PMID: 39627315
25. Gatica M, Atkinson-Clement C, Mediano PAM, Alkhawashki M, Ross J, Sallet J, et al. Transcranial ultrasound stimulation effect in the redundant and synergistic networks consistent across macaques. Netw Neurosci. 2024;8(4):1032–50. https://doi.org/10.1162/netn_a_00388 PMID: 39735508
26. Williams PL, Beer RD. Nonnegative decomposition of multivariate information. arXiv preprint 2010. https://arxiv.org/abs/1004.2515
27. Rosas F, Mediano PAM, Ugarte M, Jensen HJ. An information-theoretic approach to self-organisation: emergence of complex interdependencies in coupled dynamical systems. Entropy (Basel). 2018;20(10):793. https://doi.org/10.3390/e20100793 PMID: 33265882
28. Mediano PAM, Rosas FE, Luppi AI, Carhart-Harris RL, Bor D, Seth AK. Towards an extended taxonomy of information dynamics via Integrated Information Decomposition. 2021.
29. Seguin C, van den Heuvel MP, Zalesky A. Navigation of brain networks. Proc Natl Acad Sci U S A. 2018;115(24):6297–302. https://doi.org/10.1073/pnas.1801351115 PMID: 29848631
30. Avena-Koenigsberger A, Misic B, Sporns O. Communication dynamics in complex brain networks. Nat Rev Neurosci. 2017;19(1):17–33. https://doi.org/10.1038/nrn.2017.149 PMID: 29238085
31. Estrada E, Gómez-Gardeñes J, Lacasa L. Network bypasses sustain complexity.Proceedings of the National Academy of Sciences of the United States of America. 2023;120. https://doi.org/10.1073/pnas

32. Kaiser M, Hilgetag CC. Modelling the development of cortical systems networks. Neurocomputing. 2004;58–60:297–302. https://doi.org/10.1016/j.neucom.2004.01.059
33. Kaiser M, Hilgetag CC. Nonoptimal component placement, but short processing paths, due to long-distance projections in neural systems. PLoS Comput Biol. 2006;2(7):e95. https://doi.org/10.1371/journal.pcbi.0020095 PMID: 16848638
34. Hayward CJ, Huo S, Chen X, Kaiser M. Nonoptimal component placement of the human connectome supports variable brain dynamics. Netw Neurosci. 2023;7(1):254–68. https://doi.org/10.1162/netn_a_00282 PMID: 37334003
35. Goñi J, van den Heuvel MP, Avena-Koenigsberger A, Velez de Mendizabal N, Betzel RF, Griffa A, et al. Resting-brain functional connectivity predicted by analytic measures of network communication. Proc Natl Acad Sci U S A. 2014;111(2):833–8. https://doi.org/10.1073/pnas.1315529111 PMID: 24379387
36. Seguin C, Jedynak M, David O, Mansour S, Sporns O, Zalesky A. Communication dynamics in the human connectome shape the cortex-wide propagation of direct electrical stimulation. Neuron. 2023;111(9):1391-1401.e5. https://doi.org/10.1016/j.neuron.2023.01.027 PMID: 36889313
37. Deco G, Cruzat J, Cabral J, Tagliazucchi E, Laufs H, Logothetis NK, et al. Awakening: predicting external stimulation to force transitions between different brain states. Proc Natl Acad Sci U S A. 2019;116(36):18088–97. https://doi.org/10.1073/pnas.1905534116 PMID: 31427539
38. Cofré R, Herzog R, Mediano PAM, Piccinini J, Rosas FE, Perl YS. Whole-brain models to explore altered states of consciousness from the bottom up. 2020.
39. Gatica M, E Rosas F, A M Mediano P, Diez I, P Swinnen S, Orio P, et al. High-order functional redundancy in ageing explained via alterations in the connectome in a whole-brain model. PLoS Comput Biol. 2022;18(9):e1010431. https://doi.org/10.1371/journal.pcbi.1010431 PMID: 36054198
40. Dagnino PC, Escrichs A, López-González A, Gosseries O, Annen J, Sanz Perl Y, et al. Re-awakening the brain: forcing transitions in disorders of consciousness by external in silico perturbation. PLoS Comput Biol. 2024;20(5):e1011350. https://doi.org/10.1371/journal.pcbi.1011350 PMID: 38701063
41. Kringelbach ML, Cruzat J, Cabral J, Knudsen GM, Carhart-Harris R, Whybrow PC, et al. Dynamic coupling of whole-brain neuronal and neurotransmitter systems. Proc Natl Acad Sci U S A. 2020;117(17):9566–76. https://doi.org/10.1073/pnas.1921475117 PMID: 32284420
42. Williams PL, Beer RD. Nonnegative decomposition of multivariate information. arXiv preprint 2010. https://arxiv.org/abs/1004.2515
43. Barrett AB. Exploration of synergistic and redundant information sharing in static and dynamical Gaussian systems. Phys Rev E Stat Nonlin Soft Matter Phys. 2015;91(5):052802. https://doi.org/10.1103/PhysRevE.91.052802 PMID: 26066207
44. Luppi AI, Mediano PAM, Rosas FE, Holland N, Fryer TD, O'Brien JT, et al. A synergistic core for human brain evolution and cognition. Nat Neurosci. 2022;25(6):771–82. https://doi.org/10.1038/s41593-022-01070-0 PMID: 35618951
45. Latora V, Marchiori M. Efficient behavior of small-world networks. Phys Rev Lett. 2001;87(19):198701. https://doi.org/10.1103/PhysRevLett.87.198701 PMID: 11690461
46. Crofts JJ, Higham DJ. A weighted communicability measure applied to complex brain networks. J R Soc Interface. 2009;6(33):411–4. https://doi.org/10.1098/rsif.2008.0484 PMID: 19141429
47. Estrada E, Hatano N. Communicability in complex networks. Phys Rev E Stat Nonlin Soft Matter Phys. 2008;77(3 Pt 2):036111. https://doi.org/10.1103/PhysRevE.77.036111 PMID: 18517465
48. Coronel-Oliveros C, Medel V, Orellana S, Rodiño J, Lehue F, Cruzat J, et al. Gaming expertise induces meso scale brain plasticity and efficiency mechanisms as revealed by whole-brain modeling. Neuroimage. 2024;293:120633. https://doi.org/10.1016/j.neuroimage.2024.120633 PMID: 38704057
49. Spiegler A, Kiebel SJ, Atay FM, Knösche TR. Bifurcation analysis of neural mass models: Impact of extrinsic inputs and dendritic time constants. Neuroimage. 2010;52(3):1041–58. https://doi.org/10.1016/j.neuroimage.2009.12.081 PMID: 20045068
50. Ashwin P, Coombes S, Nicks R. Mathematical frameworks for oscillatory network dynamics in neuroscience. J Math Neurosci. 2016;6(1):2. https://doi.org/10.1186/s13408-015-0033-6 PMID: 26739133
51. Pfeffer T, Ponce-Alvarez A, Tsetsos K, Meindertsma T, Gahnström CJ, van den Brink RL, et al. Circuit mechanisms for the chemical modulation of cortex-wide network interactions and behavioral variability. Sci Adv. 2021;7(29):eabf5620. https://doi.org/10.1126/sciadv.abf5620 PMID: 34272245
52. Coronel-Oliveros C, Cofré R, Orio P. Cholinergic neuromodulation of inhibitory interneurons facilitates functional integration in whole-brain models. PLoS Comput Biol. 2021;17(2):e1008737. https://doi.org/10.1371/journal.pcbi.1008737 PMID: 33600402

53. Perl YS, Zamora-Lopez G, Montbrió E, Monge-Asensio M, Vohryzek J, Fittipaldi S, et al. The impact of regional heterogeneity in whole-brain dynamics in the presence of oscillations. Netw Neurosci. 2023;7(2):632–60. https://doi.org/10.1162/netn_a_00299 PMID: 37397876
54. Rubinov M, Sporns O. Complex network measures of brain connectivity: uses and interpretations. Neuroimage. 2010;52(3):1059–69. https://doi.org/10.1016/j.neuroimage.2009.10.003 PMID: 19819337
55. Avena-Koenigsberger A, Yan X, Kolchinsky A, van den Heuvel MP, Hagmann P, Sporns O. A spectrum of routing strategies for brain networks. PLoS Comput Biol. 2019;15(3):e1006833. https://doi.org/10.1371/journal.pcbi.1006833 PMID: 30849087
56. Shamli Oghli Y, Grippe T, Arora T, Hoque T, Darmani G, Chen R. Mechanisms of theta burst transcranial ultrasound induced plasticity in the human motor cortex. Brain Stimul. 2023;16(4):1135–43. https://doi.org/10.1016/j.brs.2023.07.056 PMID: 37524296
57. Alexander GE, DeLong MR, Strick PL. Parallel organization of functionally segregated circuits linking basal ganglia and cortex. Annu Rev Neurosci. 1986;9:357–81. https://doi.org/10.1146/annurev.ne.09.030186.002041 PMID: 3085570
58. Hwang K, Bertolero MA, Liu WB, D'Esposito M. The human thalamus is an integrative hub for functional brain networks. J Neurosci. 2017;37(23):5594–607. https://doi.org/10.1523/JNEUROSCI.0067-17.2017 PMID: 28450543
59. Greene DJ, Marek S, Gordon EM, Siegel JS, Gratton C, Laumann TO, et al. Integrative and network-specific connectivity of the basal ganglia and thalamus defined in individuals. Neuron. 2020;105(4):742-758.e6. https://doi.org/10.1016/j.neuron.2019.11.012 PMID: 31836321
60. Shine JM, Lewis LD, Garrett DD, Hwang K. The impact of the human thalamus on brain-wide information processing. Nat Rev Neurosci. 2023;24(7):416–30. https://doi.org/10.1038/s41583-023-00701-0 PMID: 37237103
61. Pathak A, Roy D, Banerjee A. Whole-brain network models: from physics to bedside; 2022.
62. Zeng K, Li Z, Xia X, Wang Z, Darmani G, Li X, et al. Effects of different sonication parameters of theta burst transcranial ultrasound stimulation on human motor cortex. Brain Stimul. 2024;17(2):258–68. https://doi.org/10.1016/j.brs.2024.03.001 PMID: 38442800
63. Caffaratti H, Slater B, Shaheen N, Rhone A, Calmus R, Kritikos M, et al. Neuromodulation with ultrasound: hypotheses on the directionality of effects and community resource. medRxiv. 2025:2024.06.14.24308829. https://doi.org/10.1101/2024.06.14.24308829 PMID: 38947047
64. Lynn CW, Bassett DS. The physics of brain network structure, function and control. Nat Rev Phys. 2019;1(5):318–32. https://doi.org/10.1038/s42254-019-0040-8
65. Camino-Pontes B, Diez I, Jimenez-Marin A, Rasero J, Erramuzpe A, Bonifazi P, et al. Interaction information along lifespan of the resting brain dynamics reveals a major redundant role of the default mode network. Entropy (Basel). 2018;20(10):742. https://doi.org/10.3390/e20100742 PMID: 33265831
66. Gatica M, Cofré R, Mediano PAM, Rosas FE, Orio P, Diez I, et al. High-order interdependencies in the aging brain. Brain Connect. 2021;11(9):734–44. https://doi.org/10.1089/brain.2020.0982 PMID: 33858199
67. Varley TF, Sporns O, Stevenson NJ, Welch MG, Myers MM, Vanhatalo S, et al. Emergence of a synergistic scaffold in the brains of human infants. Cold Spring Harbor Laboratory; 2024. http://dx.doi.org/10.1101/2024.02.23.581375
68. Herzog R, Rosas FE, Whelan R, Fittipaldi S, Santamaria-Garcia H, Cruzat J, et al. Genuine high-order interactions in brain networks and neurodegeneration. Neurobiol Dis. 2022;175:105918. https://doi.org/10.1016/j.nbd.2022.105918 PMID: 36375407
69. Hindriks R, Broeders TAA, Schoonheim MM, Douw L, Santos F, van Wieringen W, et al. Higher-order functional connectivity analysis of resting-state functional magnetic resonance imaging data using multivariate cumulants. Hum Brain Mapp. 2024;45(5):e26663. https://doi.org/10.1002/hbm.26663 PMID: 38520377
70. Luppi AI, Mediano PAM, Rosas FE, Allanson J, Pickard JD, Carhart-Harris RL, et al. A synergistic workspace for human consciousness revealed by integrated information decomposition. eLife Sciences Publications, Ltd.; 2023. http://dx.doi.org/10.7554/elife.88173.1
71. Varley TF, Pope M, Puxeddu MIG, Faskowitz J, Sporns O. Partial entropy decomposition reveals higher-order information structures in human brain activity. Proceedings of the National Academy of Sciences of the United States of America. 2023;120. https://doi.org/10.1073/pnas
72. Finn C, Lizier JT. Pointwise partial information decomposition using the specificity and ambiguity lattices. Entropy (Basel). 2018;20(4):297. https://doi.org/10.3390/e20040297 PMID: 33265388
73. Ince R. Measuring multivariate redundant information with pointwise common change in surprisal. Entropy. 2017;19(7):318. https://doi.org/10.3390/e19070318